remote sensing

MDPI

Article

Sea Level Rise, Land Subsidence, and Flood Disaster Vulnerability Assessment: A Case Study in Medan City, Indonesia

Jonson Lumban-Gaol [1,*], Josaphat Tetuko Sri Sumantyo [2,3], Efendy Tambunan [4], David Situmorang [1], I Made Oka Guna Antara [2], Maya Eria Sinurat [1], Ni Putu Asri Ratna Suhita [1], Takahiro Osawa [5] and Risti Endriani Arhatin [1]

[1] Department of Marine Science and Technology, Faculty of Fisheries and Marine Science, IPB University, Bogor 16680, Indonesia; david_situmorang@apps.ipb.ac.id (D.S.); maya_eria@apps.ipb.ac.id (M.E.S.); ratnasuhita@apps.ipb.ac.id (N.P.A.R.S.); risti@apps.ipb.ac.id (R.E.A.)
[2] Center for Environmental Remote Sensing, Chiba University, Chiba 263-8522, Japan; jtetukoss@faculty.chiba-u.jp or jtetukoss@staff.uns.ac.id (J.T.S.S.); oka@unud.ac.id (I.M.O.G.A.)
[3] Department of Electrical Engineering, Faculty of Engineering, Universitas Sebelas Maret, Surakarta 57126, Indonesia
[4] Department of Civil Engineering, Faculty of Engineering, Universitas Kristen Indonesia, Jakarta 13630, Indonesia; efendy.tambunan@uki.ac.id
[5] Centre for Research and Application of Satellite Remote Sensing (YUCARS), Yamaguchi University, Ube 755-0097, Japan; osawaunu@yamaguchi-u.ac.jp
* Correspondence: jonsonlumban@apps.ipb.ac.id

Abstract: Global sea level rise (SLR) has emerged as a pressing concern because of its impacts, especially increased vulnerability of coastal urban areas flooding. This study addresses the pressing concern of SLR and flood vulnerability in the East Coast of North Sumatra (ECNS) and Medan City. We employ a data-driven approach integrating multicriteria analysis, analytical hierarchy process (AHP)-based weighting, and spatial modeling within a geographic information system framework. The analysis considers crucial factors such as slope, land use, soil type, SLR, and land deformation. The study expands the existing framework by incorporating SLR and land subsidence, acknowledging their significant roles in exacerbating flood vulnerability. Future flood-intensity scenarios are simulated based on SLR projections. Data for spatial analysis primarily originated from multisensor satellite imagery, secondary sources from published literature, and field surveys. We validated the consistency of the variable weightings assigned for vulnerability analysis using a consistency ratio threshold (<0.1). Finally, the established flood vulnerability model was validated by comparing its predictions with recorded flood events in the ECNS and Medan City. The ECNS and Medan City areas were classified as very high and highly vulnerable to flooding, respectively.

Keywords: AHP; DInSAR; disaster; flood; GIS; land subsidence; satellite; sea level rise

Citation: Lumban-Gaol, J.; Sumantyo, J.T.S.; Tambunan, E.; Situmorang, D.; Antara, I.M.O.G.; Sinurat, M.E.; Suhita, N.P.A.R.; Osawa, T.; Arhatin, R.E. Sea Level Rise, Land Subsidence, and Flood Disaster Vulnerability Assessment: A Case Study in Medan City, Indonesia. *Remote Sens.* **2024**, *16*, 865. https://doi.org/10.3390/rs16050865

Academic Editors: Bruno Adriano, Martina Zeleňáková, Jiaguang Li, Omid Ghorbanzadeh and Mohammadtaghi Avand

Received: 31 October 2023
Revised: 22 February 2024
Accepted: 22 February 2024
Published: 29 February 2024

1. Introduction

The observed trends in the global mean sea level (GMSL) reveal a significant increase of 3.2 ± 0.4 mm year^{-1} over the past few decades [1]. However, this rate of change exhibits pronounced regional variability. For instance, the Vietnam Sea has experienced a GMSL rise exceeding 5 mm year^{-1}, whereas the South China and Java Seas have experienced GMSL rates of approximately 4 and 5 mm year^{-1}, respectively [2–4]. These regional disparities highlight the critical need for localized assessments of the impacts of sea level rise (SLR). SLR poses a significant threat to coastal environments, with a cascading effect on various environmental conditions. Increased frequency and intensity of extreme coastal flooding, coupled with coastal erosion and saltwater intrusion into freshwater aquifers, are just a few of the environmental consequences of SLR [5,6]. Furthermore, rising sea levels,

when combined with storm surges, exacerbate the threat of coastal flooding, threatening crucial aspects of human life [7,8]. Tens of millions of people residing in coastal regions of developing nations are particularly vulnerable to displacement due to SLR and its associated economic and ecological consequences [9]. Studies estimate that global economic losses due to SLR-induced floods could range from 0.3% to 9.3% of GDP [10]. For example, research in Bangkok predicts a 1.5-fold increase in flood impacts in 2100 [11]. In fact, current efforts to minimize flood impacts have demonstrated inadequate results. Studies in Israel highlight the need for stronger flood management policies [12]. These findings underscore the critical need for adaptation strategies to address the escalating social and economic losses from flood disasters, amplified by SLR [11]. Therefore, assessing the flood vulnerability in densely populated coastal cities is important for informing effective adaptation strategies.

Beyond the global phenomenon of SLR, local-scale land subsidence, driven by vertical land movements (uplift/subsidence), tectonic and volcanic activity, sediment loading, and groundwater pumping, can produce significant variations in relative sea level [13]. Consequently, accounting for land subsidence and SLR becomes essential for accurately assessing the vulnerability of coastal areas, especially urban areas, to flooding.

Several studies have demonstrated the critical connection between land subsidence and the exacerbation of flooding events, especially in big cities in Vietnam, Italy (e.g., the Mediterranean) [14–16], and Indonesia (e.g., Bandung [17], Jakarta [18], and Semarang [19]). Land subsidence makes urban areas vulnerable as a very large proportion of the population relies on wells for water supply. However, land subsidence has not generally been considered in flood hazard studies and mitigation efforts because research data on the rate of land subsidence are limited.

Some researchers have developed several methods to estimate the land deformation rate from radar satellite data, such as the differential interferometric synthetic aperture radar (DInSAR) method. DInSAR interferometry is an advanced and useful technique for detecting and monitoring deformation movements [19]. It can determine changes in the volume deformation of the soil surface [17,20,21] and the results can be compared with those of the global positioning system (GPS) survey [22]. DInSAR is an effective method for detecting ground displacement or land deformation in the antenna line-of-sight (slant-range) direction using SAR data acquired at two different times [23–26]. DInSAR complements ground-based methods, such as GPS measurements, by providing information across a large coverage area even when the location is inaccessible [27,28]. Data from the freely available Sentinel-1A satellite radar are a great source of data for generating land deformation maps.

Several studies have demonstrated that flood conditions on the East Coast of North Sumatra (ECNS) and Medan City are worsening due to several factors, such as changes in land use, deforestation in upstream areas, and increasing population [29–31]. However, no study has examined the impact of land subsidence on the risk of flooding in this area. To better predict and mitigate flooding in this area, we need accurate information about the factors contributing to flooding and its impacts.

In the global effort to mitigate disaster risk, regional assessments of vulnerability to flooding have become increasingly vital. A common method for such assessments uses Multicriteria Decision Analysis (MCDA) with Analytical Hierarchy Process (AHP) [32,33]. This approach facilitates the evaluation of numerous variables contributing to flooding, including slope, elevation, land use/land cover, drainage density, rainfall intensity, and soil type. These factors, collected and analyzed using geographic information systems (GIS), serve as the basis for mapping flood vulnerability areas [29–31]. However, each variable contributes differently to the overall flood vulnerability, requiring a weighting system. The AHP method has proven effective in assigning appropriate weights, leading to a more accurate and reliable flood vulnerability analysis [32,33].

This study presents a novel approach to flood vulnerability assessment in ECNS and Medan City by integrating MCDA with two crucial factors: SLR trend and land deforma-

tion. Previous studies focused only on variables such as slope, elevation, land use/land cover, drainage density, rainfall, and soil type; however, this study extends the existing framework by incorporating SLR and land subsidence. This extension acknowledges the significant role of these factors in exacerbating flood vulnerability, especially in coastal regions. The integration of SLR and land subsidence into this framework will generate a more comprehensive and accurate assessment of flood vulnerability. This enhanced understanding will be considered in developing effective flood disaster management strategies for ECNS and Medan City, ultimately contributing to the safety and well-being of local communities.

Study Site

The study site is located on the ECNS and Medan City (03°39′00″S–98°38′00″E to 03°53′00″S–98°58′00″E). The ECNS and Medan City cover 265 km^2 and have 21 subdistricts (Figure 1). The study area is growing rapidly, as evidenced by the expansion of settlements and the physical development of the city area. The increase in population [34] and development has led to the conversion of vegetated land for other purposes, such as economic areas and settlements.

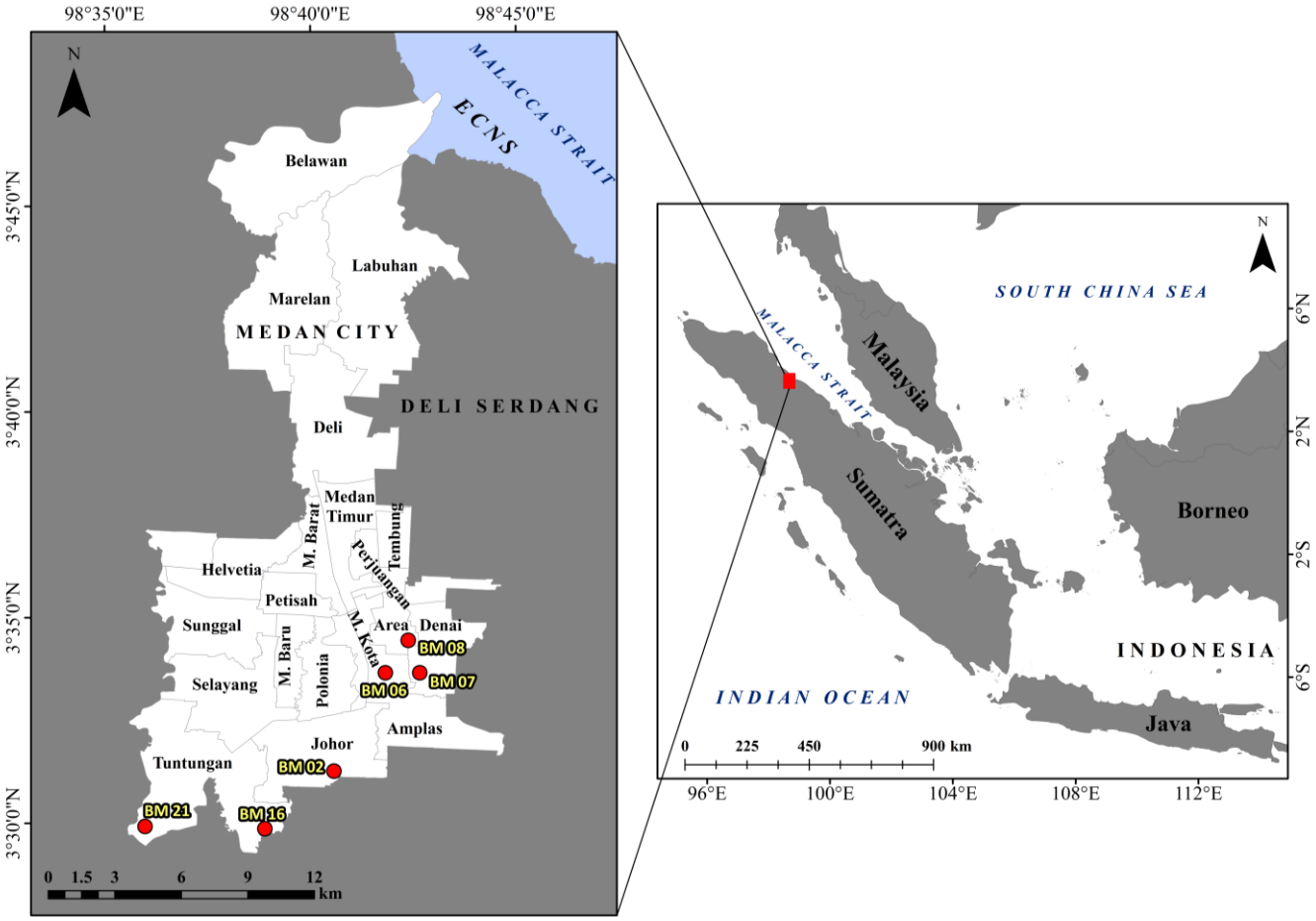

Figure 1. Study site and distribution of benchmarks in ECNS and Medan City.

Medan City, the capital city of North Sumatra Province, has a population of 2.4 million people with an area of 26,510 ha, or 3.6% of the total area. North Sumatra Province is the fifth most populous and the third largest city in Indonesia. It is a sloping lowland starting from Belawan City, located on the ECNS. It is located at the confluence of two rivers, the Deli and Babura, which flow into Belawan beach. Flooding tends to occur during heavy rainfall and worsens at high tide. Flooding in ECNS and Medan City occurs every

year. Recently, every time there has been heavy rain, Medan City has experienced flooding (Table 1).

Table 1. Annual occurrence of flooding on the East Coast of North Sumatra and Medan City (2020–2023).

Time	Damage Caused by Flooding	Image
3 December 2020	A significant flooding impacted the city of Medan, Indonesia, affecting 5965 people. Water levels reached alarming heights of 3–5 m. The National Disaster Management Agency confirmed that five people tragically lost their lives, whereas two remain missing. The floodwaters impacted four subdistricts within Medan City: Medan Johor, Medan Maimun, Medan Sunggal, and Medan Tuntungan.	 Photo: BPBD Medan City (04/12/2020).
7 December 2021	A tidal flooding affected 60,102 people in Belawan and Medan, Indonesia. The high sea tides triggered ("Rob" in local terminology) flood inundated several subdistricts within the administrative areas of Medan and Belawan Districts. Six subdistricts were affected: Belawan I, Belawan II, Sicanang, Bahari, Bahagia, and Bagan Deli.	 Photo: BPBD Belawan- Medan City (17/12/2021).
27 February 2022	A significant flooding affected 3267 residential houses in Medan, Indonesia. Water levels ranged from 30 cm to 1 m, with some areas in Kampung Aur experiencing flood heights exceeding 2 m. The flood impacted nine subdistricts: Medan Johor, Medan Selayang, Medan Maimun, Medan Baru, Medan Sunggal, Medan Polonia, Medan Denai, Medan Labuhan, and Medan Amplas.	 Photo: BPBD Medan City (27/02/2022).
3 September 2023	A significant flooding impacted 346 residential houses in Medan City, Indonesia. The floodwaters submerged houses on Perjuangan and Dwikora Streets, Tanjung Rejo Village, Medan Sunggal District. Additionally, residents residing on Karya Dalam Street, Rukun Street, Ayem Street, and Sepakat Street in Karang Berombak Village, West Medan District, were also affected by floodwater inundation.	 Photo: BPBD Medan City (03/09/2023).

2. Materials and Methods

In this study, we employed a multisensor satellite data approach coupled with field surveys. Data processing and analysis were conducted using a combination of different types of software, including the Sentinel Application Platform (SNAP) v9.0.0, MATLAB R2023b v23.2, and QGIS v3.28.15 'Firenze'. Field surveys were conducted thrice, in September 2016, September 2022, and October 2023, to measure coastal slope by placing a water-level device, land use, and benchmark (BM) point height, respectively.

2.1. Satellite-Derived Land Deformation

SAR data from the Sentinel-1 satellite (https://asf.alaska.edu/, accessed on 10 November 2022) was used to analyze land deformation. SAR Sentinel-1A Level 1 single look complex (SLC) imagery and digital elevation model (DEM) data were used to estimate the rate of land subsidence. We collected Sentinel-1A SAR data in 2016 and 2017 from vertical-transmit and vertical-received (VV) polarization data in the ascending mode and Sentinel-1A VV polarization data in the ascending mode (incidence pixel distance 14.1 m).

SAR image data were processed images in the SNAP software using the DInSAR method with the calculation of the phase difference of two or more SAR [35]. DInSAR extracts the total phase caused by deforming/changing ground values by eliminating or reducing other factors contributing to the formation of phase interferograms. The DInSAR technique allows terrain displacement to be calculated as the interferometric phase containing the following phase terms [35]:

$$\Delta\varphi d = \frac{4\pi}{\lambda}\,\Delta R \tag{1}$$

with the projection of the relative point displacement onto the radar lens of sight (LOS). In particular, the variation in the interferometric phase can be mathematically represented by the following equation [35]:

$$\Delta\varphi = \Delta\varphi d + \Delta\varphi topo + \Delta\varphi orb + \Delta\varphi atm + \Delta\varphi n, \tag{2}$$

where $\Delta\varphi d$ accounts for the possible displacement of the scatterer between observations, $\Delta\varphi topo$ represents the residual topography-induced phase due to nonperfect knowledge of the height profile (i.e., DEM errors), $\Delta\varphi orb$ accounts for inaccurate orbital information in the synthesis of the topographic phase, $\Delta\varphi atm$ denotes the phase components due to the change in the atmospheric and ionospheric dielectric constant between the master/slave acquisitions, and $\Delta\varphi n$ accounts for decorrelation phenomena (e.g., spatial, temporal, and thermal).

In the following section, we analyze some fundamental steps and critical aspects of interferometric processing.

Coregistration of SAR images is necessary to align the images so that they can be pixel-wise compared to detect changes in the scene. The coherence between the master and slave images is given as follows [35]:

$$\gamma = \frac{E[\mathrm{u1u2}*]}{\sqrt{E[(\mathrm{u1u1}*)E(\mathrm{u2u2}*)}}, 0 \le \gamma \le 1 \tag{3}$$

where $E\,[\cdot]$ represents the statistical expectation and u1 and u2 represent the two images. The coefficient values (γ) range from 0 (low coherence) to 1 (high coherence).

The next step is phase unwrapping, which is performed using a statistical cost network flow algorithm for phase unwrapping developed at Stanford University (SNAPHU v2.0.6). Unwrap data conversion from phase form to elevation value is performed to determine the difference in height using the DInSAR process or convert from slant to height using the phase-to-displacement tools in the SNAP v9.0.0 software. Figure 2 shows the flowchart of the data processing.

2.2. In Situ Land Deformation Measurement

In this study, we employed in situ land deformation measurements using geodetic GPS to compare with land deformation patterns observed by SAR satellites. Due to data availability constraints, GPS altitude point data from 2010 were used as the reference point for displacement analysis. The land surface deformation data presented in this study encompass measurements conducted in 2010 and 2023. GPS point height (z) measurements were conducted at six BM positions (BM-02, 06, 07, 08, 14, 16, and 21), as shown in

Figure 1. These BM positions belong to the Geodetic Control Network established by the North Medan City Settlement and Spatial Planning Service, Sumatra Province, in 2010.

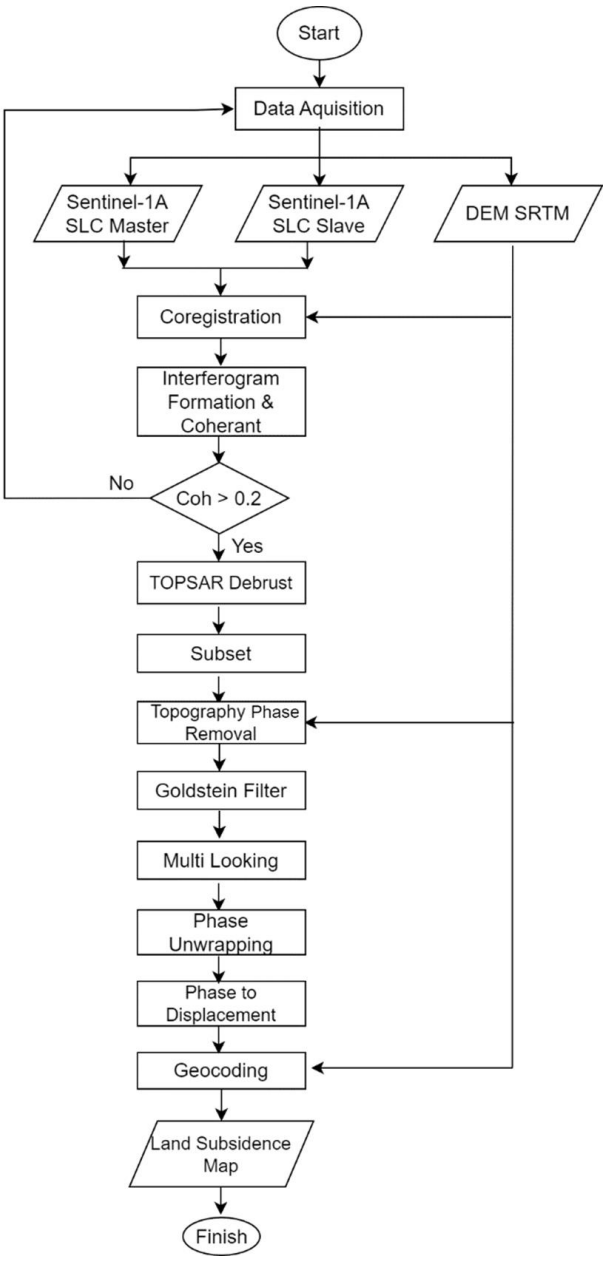

Figure 2. Flowchart of satellite data processing using the DInSAR method with the SNAP software.

Field observations and GPS height (z) data collection were conducted in September 2023. Each GPS BM was surveyed using a Geodetic GPS employing the Real-Time Kinematic-Networked Transport of Radio Technical Commission for Maritime Services (RTCM) via Internet Protocol Real-Time Kinematic-Networked Transport (RTK-NTRIP) of the RTCM method. This method employs the Indonesia Continuously Operating Reference Station operated by the Indonesian Geospatial Information Agency (INA-CORS BIG) located in Medan and Belawan as reference points. Several references confirm that the accuracy and precision of GPS measurements using the RTK-NTRIP method with INA-CORS BIG are within acceptable standards and meet relevant requirements (Figure 3). The survey equipment included CHCNAV i50 Geodetic GPS/Global Navigation Satellite System (GNSS) Receivers, with the following specifications: horizontal accuracy: 8 mm + 1 ppm-RMS, vertical accuracy: 15 mm + 1 ppm-RMS, Initialization time: <10 s, and Initialization reliability: >99.9%.

Figure 3. Several BM positions in Medan City during the survey in September 2023.

2.3. Sea Level Rise Trends

Sea level time series data in the ECNS were the monthly gridded 0.25° × 0.25° sea level anomaly (SLA) in the period of 1993–2021 (29 years) distributed by the Copernicus Marine Environment Monitoring Service (CMEMS). Details of the dataset can be found at https://doi.org/10.48670/moi-00148 (accessed on 18 November 2022). The global SLR trends based on satellite altimetry data released by the Colorado University Sea Level Group can be accessed at https://sealevel.colorado.edu/files/2023_rel2/gmsl_2023rel2_seasons_rmvd.txt (accessed on 4 December 2023). Sea level projections through the 21st century for representative concentration pathway (RCP) 4.5 and RCP 8.5 are collected by Climate Econometric at the following URL: http://www.climateeconometrics.org/sealevel_rcp/ (accessed on 27 November 2023) [36,37].

2.4. Land Use, Soil Type, and Slope

This study incorporates several additional variables beyond land deformation and SLR trends to comprehensively assess flood vulnerability. These include land use, soil type, and slope. The land use map produced by the North Sumatra Regional Development Planning Agency has been updated with Google Earth delineations. The soil type map was extracted from the existing literature [31] and land slope map [38]. However, direct field measurements using the leveling method were employed for improved accuracy.

2.5. Spatial Analysis of Flood Disaster Vulnerability

Vulnerability is defined as a complex interplay of physical, social, economic, and environmental factors that influence the level of potential damage from hazards caused by a disaster [39]. In Medan City, we unraveled the vulnerability by analyzing a web of physical parameters: slope, land use, land subsidence, SLR, and soil type. The AHP technique is a multicriteria decision-making approach developed by Saaty [40,41]. The AHP technique helps us to assess the relative importance of various parameters that influence flood vulnerability.

The core principles of AHP can be categorized into four key stages: problem hierarchy, criteria and alternative evaluation, priority setting, and logical consistency. The AHP procedure is described as follows. First, the decision problem is decomposed into a hierarchical structure. This structure organizes the goal and various vulnerability components, facilitating a clear and organized analysis. Then, a pairwise comparison employs a nine-point scale and expert elicitation. The scale permitted assigning a value of "1" (usually in the main diagonal) when two criteria possess equal priority.

The next step is the analysis of the pairwise comparison. Each pairwise comparison matrix undergoes a normalization process. This typically involves dividing each element in the matrix by the sum of its corresponding row, resulting in a matrix in which each row sums to one.

The normalized matrix is then subjected to eigenvector analysis by applying the geometric mean of the rows. To ensure and validate the AHP results, a consistency ratio (CR) is calculated. The CR value below a predefined threshold (<0.1) indicates acceptable consistency, suggesting reliable and valid weights. If the CR value exceeds this threshold, the decision maker revisits the pairwise comparisons and revises their judgments. Equation (4) presents a mathematical formula for measuring the CR, where CI is the consistency index and RI is the random index. The RI is the random index associated with generated comparison matrices of a specific size. In the case of a matrix size of 5, an RI value of 1.12 is suggested.

$$CR = \frac{CI}{RI} \tag{4}$$

Mathematically, the CI value is calculated as follows:

$$CI = \frac{(\lambda_{max} - n)}{(n-1)}, \tag{5}$$

where λ_{max} represents the maximum eigenvalue of the matrix and n represents the number of factors or alternative choices [40,41].

The spatial model of flood vulnerability is implemented using a model builder in QGIS, which is built based on the MCDA procedure. Each criterion is given a relative importance weight based on the AHP method. The total score Flood Vulnerability Index (FVI)(xi) is the sum of each criterion by multiplying the weight by the scale value of the criterion as follows:

$$FVI(x_i) = \sum_j w_j r_{ij} \tag{6}$$

where w_j is a normalized weight such that $\Sigma w_j = 1$ and r_{ij} is the attribute transformed into the comparable scale. The weights represent the relative importance of the attributes. The most preferred alternative is selected by identifying the maximum value of FVI(x_i) for $i = 1, 2, \ldots, m$.

To integrate AHP with GIS analysis in flood vulnerability mapping, Figure 4 presents a conceptual framework for the proposed approach. The depicted steps include primary data collection, its manipulation in a GIS environment, and MCDA. These steps can be categorized as processing and analyzing spatial datasets for flood vulnerability analysis.

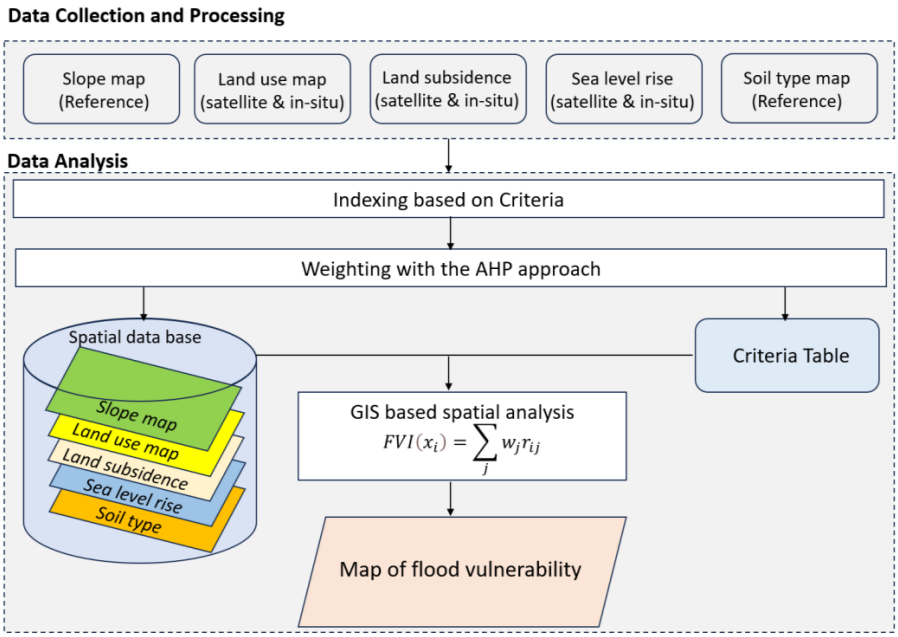

Figure 4. Multicriteria Decision Analysis conceptual framework for analytical hierarchy-process-geographic information system base flood mapping vulnerability.

3. Results

3.1. Trends in Sea Level Rise and Coastal Flooding

The satellite-derived sea surface height anomaly data revealed a significant trend of SLR ECNS waters exceeding 4.79 mm year^{-1} (Figure 5a). This rate is notably higher than the global average SLR (Figure 5b) [42,43] and the average SLR in Indonesian waters [44,45]. The evaluation of altimetry data products with tide gauges shows excellent performance for monitoring sea levels with high accuracy in Indonesian waters [44]. Such an elevated SLR in the ECNS region has a high risk of flooding, especially during high tide events.

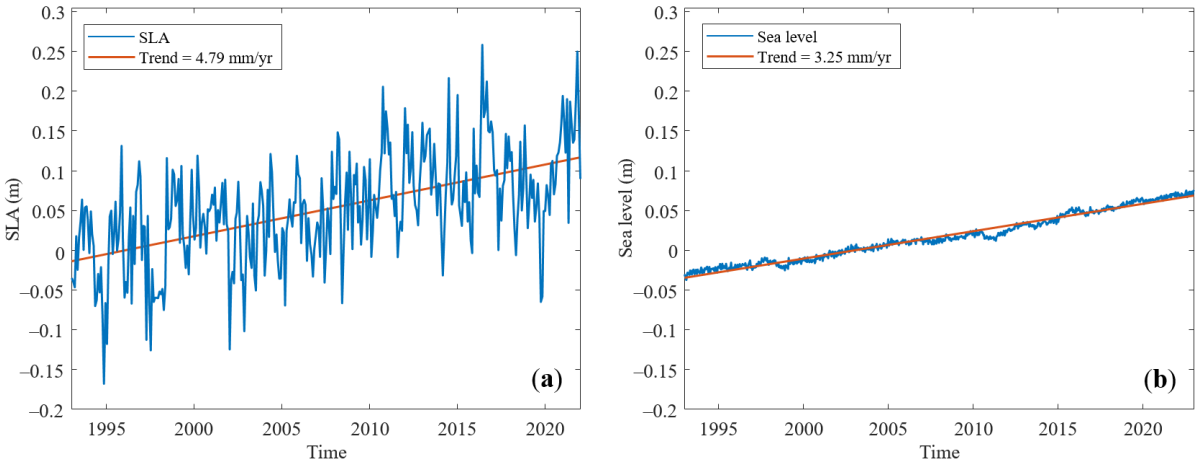

Figure 5. Trends of sea level rise on (**a**) the ECNS and (**b**) globally based on satellite altimetry data from 1993 to 2022.

3.2. Land Subsidence

The analysis of the spatial planning map for Medan City reveals that trade and settlement areas dominate land use patterns. Furthermore, SAR Sentinel 1A satellite data indicate significant land subsidence along the ECNS and within Medan City, with rates ranging from −0.01 to −19.00 cm year^{-1} (Figure 6a). This spatial pattern of land subsidence velocity is consistent with existing landform characteristics [31]. Alluvial plains exhibit the highest subsidence rates, followed by tidal areas and beaches (Figure 6b). Interestingly, the area around Medan City, with its large concentration of high-rise buildings and commercial activities, experiences the most pronounced land subsidence. In contrast, areas with significant vegetation cover, such as coastal mangrove forests, exhibit the least significant subsidence rates.

Vertical deformation of the land surface from geodetic GPS measurements between 2010 and 2023 shows land surface subsidence over 13 years in Medan City ranging from −0.012 to −28.065 m (Table 2). The deformation pattern from GPS measurements is similar to the deformation data from SAR satellite data. Generally, the land surface in Medan City has decreased. The subsidence of the land surface in Medan City can also be seen from the condition of cracked buildings or sagging floors.

Table 2. Vertical deformation velocity at six benchmark positions in Medan City.

Bench Mark (BM)	Latitude (°N)	Longitude (°E)	Height (m) 2010 [46]	Height (m) 2023	Difference (m)
BM 02	3.521109	98.676373	301.517	300.775	−0.742
BM 06	3.560994	98.697191	135.706	131.486	−4.220
BM 07	3.560994	98.711181	116.972	88.907	−28.065
BM 08	3.574129	98.706511	08.902	08.903	−0.012
BM 16	3.497786	98.648354	423.142	416.095	−7.047
BM 21	3.498690	98.599782	523.906	523.392	−0.514

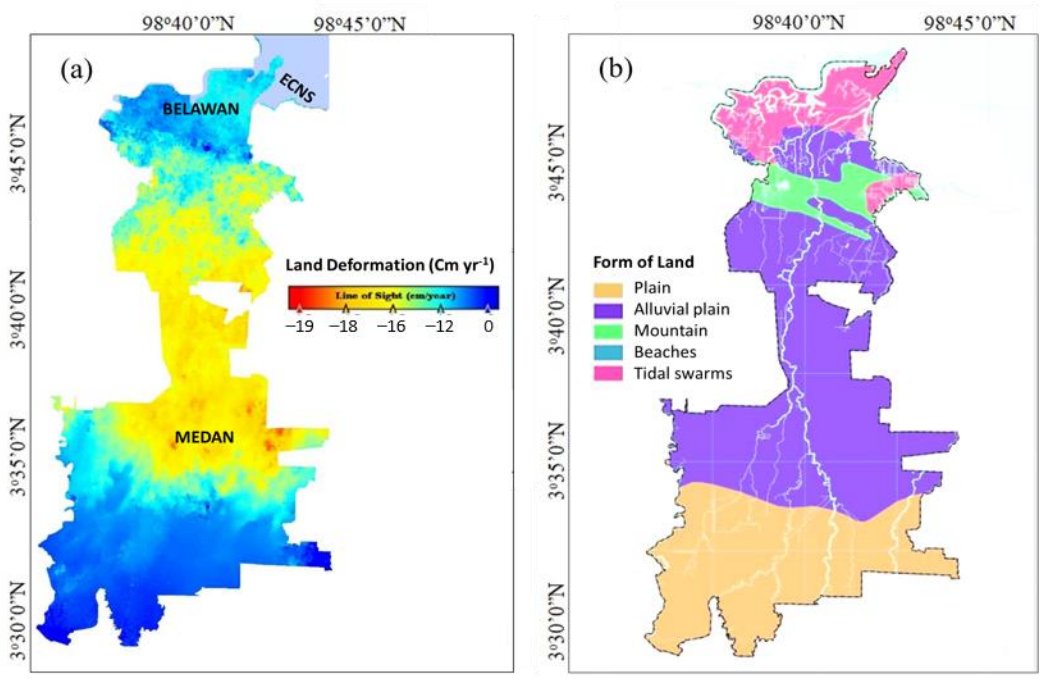

Figure 6. (**a**) Velocity of land deformation and (**b**) landform characteristics on the ECNS and Medan City [31].

3.3. Land Use, Slope, and Soil Type

Land use in Medan City consists of 11 classes (Figure 7a); the three largest classes are settlements (227,216 km^2), ponds (22,533 km^2), and mangrove forests (10,097 km^2). As the most populous city outside Java, Medan City faces a high demand for land, especially for residential development. The dominance of settlement areas, exceeding 82% of the total city area, significantly contributes to its flood vulnerability.

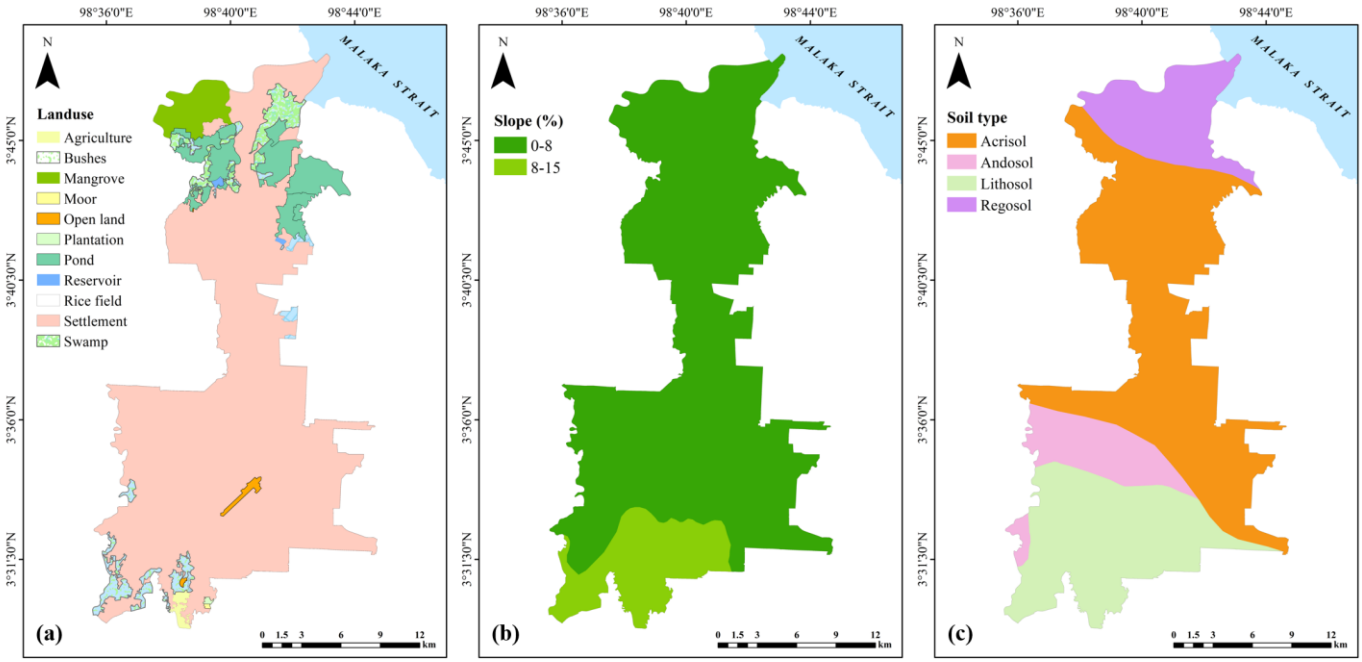

Figure 7. (**a**) Land use, (**b**) slope [38], and (**c**) soil types [31] in ECNS and Medan City.

From a topographic perspective, Medan City primarily consists of flat land, comprising approximately 90% of its total area. The remaining 10% is characterized by sloping,

predominantly ranging from 0% to 8%, with a small portion exhibiting slopes between 0% and 15% (Figure 7b). This predominantly flat landscape further amplifies the city's flood vulnerability. Interestingly, the flat topography corresponds to the dominant soil type in Medan City, which is alluvial deposits.

The analysis of soil types reveals a predominance of Acrisol, Andosol, Lithosol, and Regosol soils (Figure 7c). Acrisols are characterized by low clay accumulation and base saturation, whereas Regosols are shallow, unconsolidated soils, likely of alluvial origin. Andosols possess very low bulk densities, high water holding capacities, and variable loads. Meanwhile, Lithosols consist of shallow soil covering hard rock formations. The combined presence of Acrisol, Andosol, and Regosol soil types contributes to Medan City's flood vulnerability.

3.4. Analysis of Hierarchy Process for Flood Vulnerability

In this study, we employed the AHP approach to a multicriteria spatial analysis of flood vulnerability within the study area. We considered five physical parameters in this analysis: slope, SLR, land subsidence, land use, and soil type (Table 3). To determine the relative weights assigned to each parameter within the GIS framework, a pairwise comparison matrix was constructed. The values within each cell of this matrix were determined by expert judgment.

Table 3. Pairwise comparison matrix for the weight factors.

Variables	Slope	Sea Level Rise	Land Subsidence	Land Use	Type of Soil
Slope	1	2	2	2	2
Sea level rise	0.5	1	0.5	0.5	2
Land subsidence	0.5	2	1	0.5	2
Land use	0.5	2	2	1	2
Type of soil	0.5	0.5	0.5	0.5	1

The calculated CR of 0.043 is significantly lower than the acceptable threshold of 0.1, indicating that the pairwise comparison matrix for weighting each variable (Table 3) meets the consistency requirements specified in the AHP procedure. Table 4 presents the weights assigned to each variable based on the AHP calculations. The highest weight is attributed to the slope, followed consecutively by land use, land subsidence, SLR, and soil type. This indicates that slope is considered to be the most influential factor contributing to flood vulnerability in the study area.

Figure 7a shows the spatial distribution of flood vulnerability in Medan City, derived from the analysis of five determinant parameters with their respective weights (Table 3). The city exhibits a predominantly high (FVI: 3.41–4.20) to very high (FVI: 4.21–5.00) vulnerability classification, highlighting its significant flood vulnerability. The spatial patterns of the flood vulnerability map closely align with known areas that frequently experience flooding, such as Belawan, Marelan, Helvetia, Mandala, Citra Wisata, and Kodam. This strong correlation between vulnerability assessment and historical flood occurrence validates the effectiveness of the methodology employed (Figure 8a).

There is a strong correlation between areas classified as highly or very highly vulnerable to flooding and densely populated areas (Figure 8b). Areas classified as very high and high flood vulnerability also coincide with zones of concentrated population. This overlap highlights the increased risk posed by flooding in these densely populated areas. The presence of multiple rivers traversing Medan City, including the Bubara River, Kera River, and Seputih River, contributes significantly to its vulnerability to flooding. These rivers flow toward the coast, and their confluence with high tides, especially during heavy rainfall events, dramatically increases the risk of severe flooding.

Table 4. Criteria for each parameter in the flood vulnerability assessment of the ECNS and Medan City.

Parameter	Criteria	Level	Score	Weight
Slope (%) modified from [38]	>45	Very low	1	0.32
	26–45	Low	2	
	16–25	Moderate	3	
	9–15	High	4	
	0–8	Very high	5	
Land use [47]	Forest	Very low	1	0.24
	Plantation and bush	Low	2	
	Agriculture, rice fields, and moor	Moderate	3	
	Settlement, mixed garden, and yard crop	High	4	
	Open land, river, reservoir, and swamp	Very high	5	
Local subsidence trend (mm year^{-1}) [48]	<−1.0 Land rising	Very low	1	0.19
	−1.0–1.0	Low	2	
	1.1–2.0	Moderate	3	
	2.1–4.0	High	4	
	>4.0 Land sinking	Very high	5	
Relative sea level rise (mm year^{-1}) [49]	<1.80	Very low	1	0.14
	1.81–2.50	Low	2	
	2.51–3.00	Moderate	3	
	3.01–3.40	High	4	
	>3.4	Very high	5	
Soil type [50]		Very low	1	0.11
	Regosol and Podzolk	Low	2	
	Andosol, Lithosol, and Ferralsol	Moderate	3	
		High	4	
	Histosol, Gleysol, Vertisol, Acrisol, and Grumusol	Very high	5	

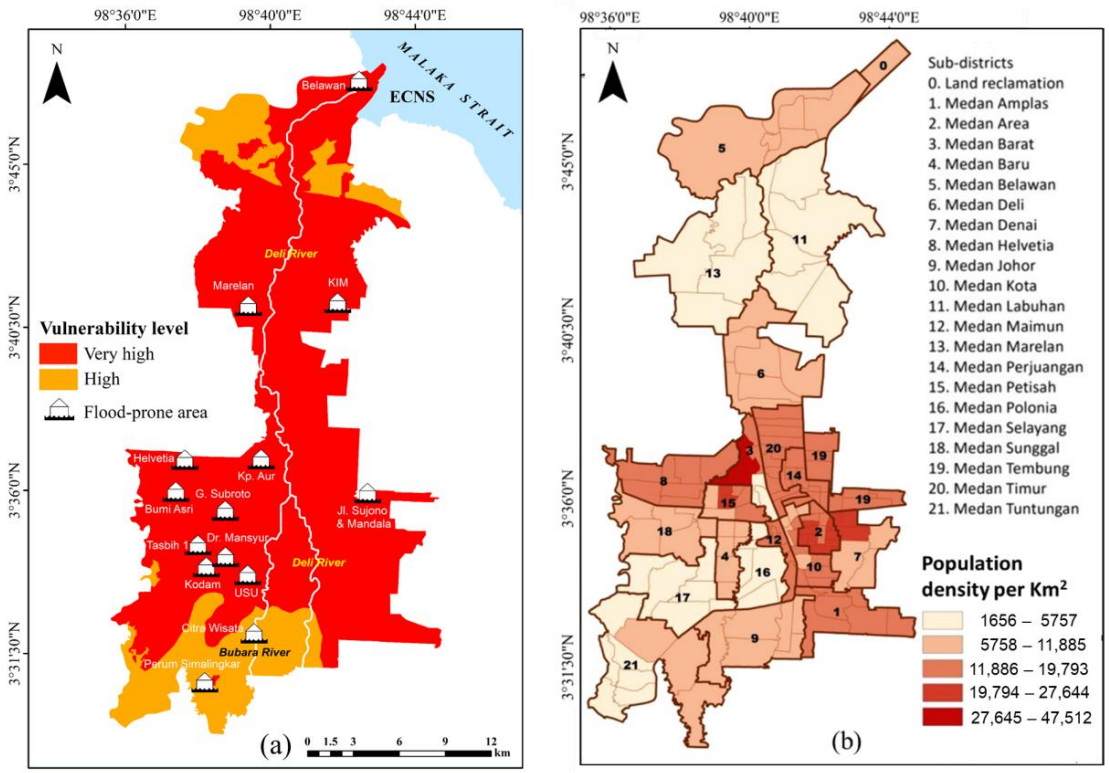

Figure 8. (**a**) Flood vulnerability map and (**b**) population density [34] in ECNS and Medan City.

4. Discussion

The findings show that ECNS experiences a significantly higher rate of SLR, exceeding the GMSL rate. The observed rate in ECNS is 4.79 mm year^{-1}, higher than the global average of 3.4 mm year^{-1}. This elevated SLR directly impacts Medan City, which is situated along the ECNS coastline and connected via the Deli River. During normal high tides, areas along the ECNS coast and Medan City remain largely safe from flooding (Figure 9a). However, during peak high tide events, the combined effect of elevated sea levels and tidal forces can trigger devastating floods. These events have damaged various buildings and disrupted economic activities along the ECNS region (Figure 9b). This flooding primarily occurs because the coastal land elevation is lower than the peak high tide level, leading to seawater overflowing and inundating coastal areas, causing significant damage to infrastructure and disrupting economic activities.

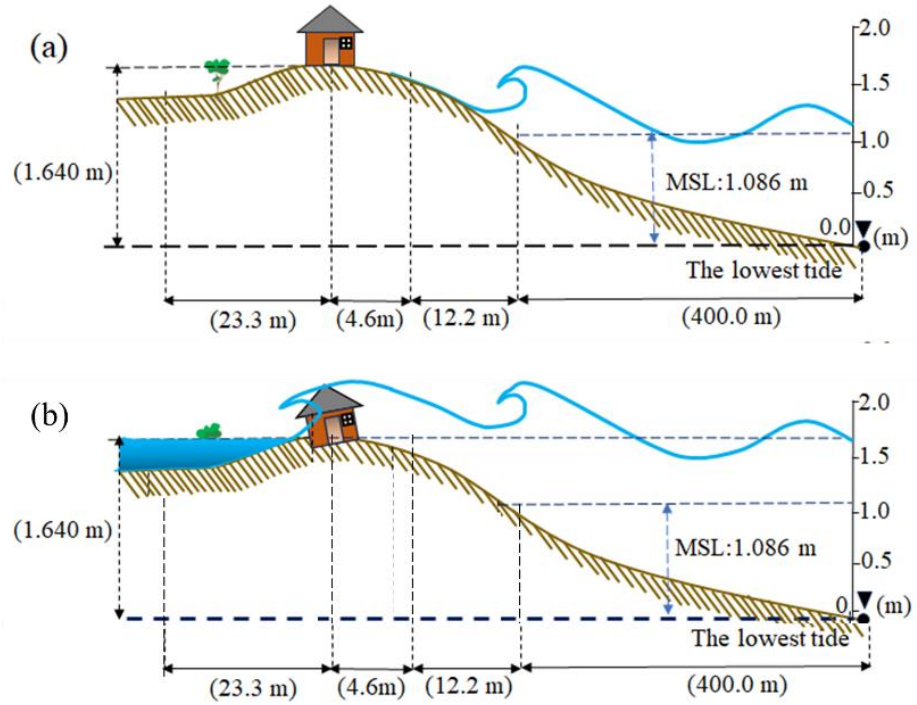

Figure 9. Coastal conditions (**a**) at normal tide (**b**) at the highest tide along ECNS.

The Intergovernmental Panel on Climate Change projects an even more alarming rate of SLR under the RCP scenarios due to intensifying ocean warming and melting glaciers and ice sheets. If substantial efforts to reduce greenhouse gas emissions are not implemented, global mean SLR is projected to range from 0.32 to 0.63 m for RCP 4.5 and 0.45 to 0.82 m for RCP 8.5 from 2081–2100 compared to the baseline period of 1986–2005 [51]. Based on these projections, ECNS could experience an SLR rate of 8–16 mm year^{-1} between 2081 and 2100 (Figure 10). This drastically elevated rate poses a significant threat to coastal communities and infrastructure in the region.

Based on the RCP 4.5 scenario, the ECNS region will experience a significant mean SLR of approximately 50 cm by 2080–2100. This dramatic increase will have a profound impact on the region, with an alarming increase in the frequency of tidal floods being one of the most prominent. Figure 10 shows the low tide variations at ECNS in December 2020. The average beach height was established as 1.64 m through leveling measurements. As a result, any high tide exceeding this height will result in beach inundation. In December 2020 alone, 20 high tide events surpassed the beach height, leading to flooding. Under the RCP 4.5 scenario, a 50-cm increase in the mean sea level by 2100 is expected to trigger an 80% surge in flood events during high tides (Figure 11). These results are consistent with findings

from previous studies, which predict that global SLR will double the frequency of extreme flooding within the next five years [7].

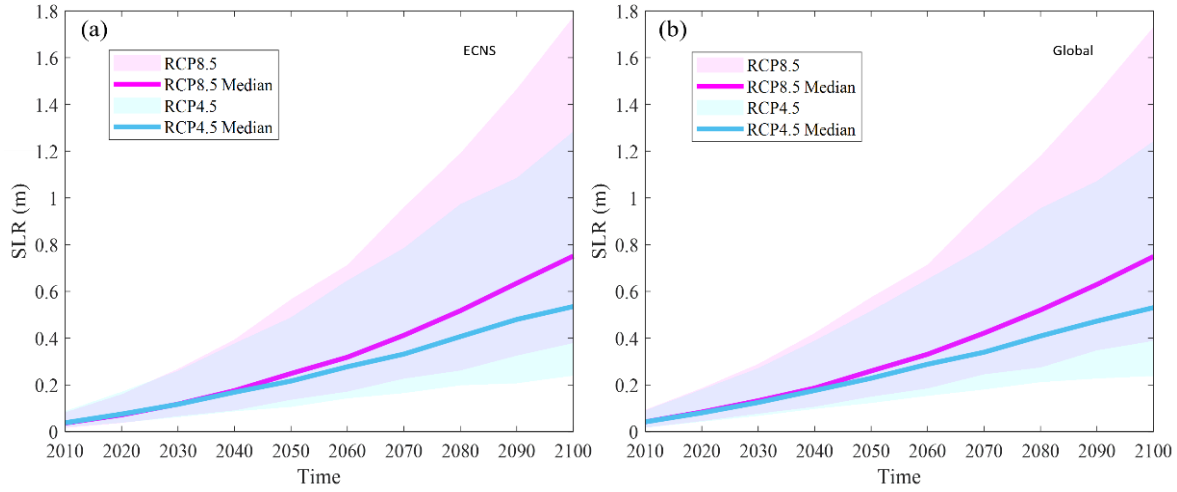

Figure 10. Sea level rise trend based on RCP 4.5 and 8.5 scenarios in (**a**) ECS and (**b**) globally.

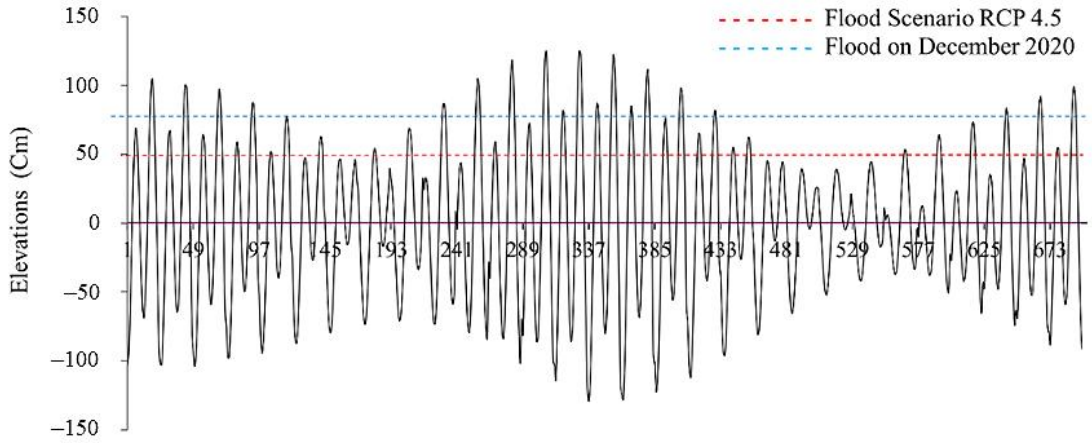

Figure 11. Tidal variations in December 2020 and flood events in ECNS.

Based on Sentinel-1 imagery and in situ measurements at several BM positions, the estimated velocity of land subsidence in the ECNS and Medan City is high. However, the field measurement data are not well distributed spatially because some measurement points have fallen or tilted. Moreover, the land subsidence pattern estimated from satellites is similar to the field measurements. These results show that Setinel-1 satellite data can be used as primary data to study land deformation in a region, especially if there are insufficient BM measurement points. This study supports previous research showing that the high quality of SAR data with precision in subcentimeter scale [25]. The land deformation velocity map shows an accuracy of 2 mm year^{-1}, even using validation procedures [52].

Despite recurring flood events, the crucial role of land subsidence in exacerbating the flood vulnerability remains largely unaddressed in ECNS and Medan City. This study revealed a spatial correlation between land subsidence rates and soil types, with Acrisol and Regosol soils exhibiting the highest subsidence, especially in coastal areas (Figure 6c). This finding resonates with the predominantly flat (0–8%) and sloping (8–15%) topography of these zones, creating an environment highly vulnerable to flood inundation (Figure 7b). The historical data on flood events further corroborate this finding, with areas experiencing frequent floods consistently overlapping with zones of high land subsidence. Field observations conducted in September 2023 in Belawan City offer visual evidence of the destructive

consequences of land subsidence. The prevalence of cracked walls and damaged floors in buildings (Figure 12a) serves as a stark reminder of the structural instability and potential safety hazards posed by this phenomenon. Furthermore, the negative impacts of SLR are readily apparent along the ECNS coastline. Rising sea water causes widespread mangrove die-off and disrupts marine ecosystems, especially around Labu Beach (Figure 12b). This environmental degradation further amplifies the vulnerability of coastal communities to flooding and other natural hazards.

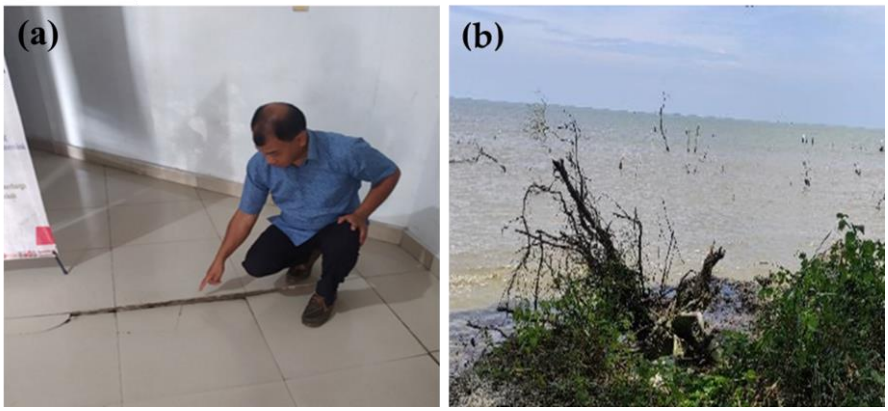

Figure 12. (**a**) Cracked building walls and falling building floors in Belawan City and (**b**) Mangrove damage and biota death at Labu Beach in ECNS based on field surveys in September 2022.

A significant correlation exists between areas of high population density and increased land subsidence rates in ECNS and Medan City [34]. This relationship is attributed to the increased demand for groundwater extraction in densely populated areas, which contributes to land subsidence [18]. The combined effects of SLR and land subsidence pose a severe threat of intensifying flood impacts in the region. This result is consistent with findings from research conducted in the Shanghai Coast area, where land subsidence and SLR were identified as the primary drivers of heightened flood risk [53].

Previous research on coastal flood vulnerability in Medan City has largely neglected the critical variables of SLR and land subsidence. This study demonstrates the significance of incorporating these factors, revealing that 80% of Medan City's area falls into the "very high" vulnerability category, exceeding the scope of previous assessments [38]. By considering the combined influence of SLR and land subsidence, we provide a more accurate and comprehensive assessment of flood vulnerability in ECNS and Medan City. This can be noted from the strong spatial correlation observed when overlaying the vulnerability map with areas prone to frequent flooding (Figure 8a). The inclusion of SLR and land subsidence as crucial variables in assessing flood potential aligns with established practices implemented by previous researchers in coastal regions [53–56].

5. Conclusions

This study examines the flood vulnerability in ECNS and Medan City by explicitly considering the critical factors of SLR and land subsidence. The observed 4.79 mm year^{-1} rate of SLR in ECNS is higher than the GMSL rate, highlighting the region's increased vulnerability to SLR-induced floods, as projected by the RCP scenario. Furthermore, the current subsidence of the region's land exacerbates future flood risks.

We integrated GIS and AHP with the MCDA approach to develop a spatial model of flood vulnerability. The model incorporates SLR and land subsidence variables and identifies more precise vulnerability classes than previous research. Specifically, 80% of the areas are classified as "very high" and 20% as "high" vulnerability areas. The weights assigned to each variable derived from AHP follow a consistent order, starting with the highest weight for slope, followed by land use, land subsidence, SLR, and soil type. The

consistency is demonstrated by a CR value of 0.04, which is well below the acceptable threshold of 0.1.

This study also emphasizes the potential of multisensor satellite data, including SAR and altimetry, as a primary data source for assessing the impact of flood disasters caused by SLR and land subsidence. The combination of wide coverage satellite spatial data with limited field data as validation will produce complete and accurate spatial data. Recognizing land subsidence and SLR as the main drivers of increasingly intense flooding provides important insights for developing effective mitigation strategies in coastal cities in Indonesia (Jakarta, Semarang, and Surabaya) and Asia, where spatial data are minimal.

Author Contributions: Conceptualization, J.L.-G., J.T.S.S., E.T. and T.O.; methodology, J.L.-G., J.T.S.S. and E.T.; software, D.S., I.M.O.G.A., M.E.S. and R.E.A.; validation, J.L.-G., J.T.S.S. and E.T.; formal analysis, J.L.-G., J.T.S.S. and E.T.; investigation, J.L.-G., J.T.S.S. and E.T.; resources, J.T.S.S. and T.O.; data curation, J.L.-G., M.E.S., N.P.A.R.S. and I.M.O.G.A.; writing—original draft preparation, J.L.-G.; writing—review and editing, J.T.S.S., E.T., N.P.A.R.S. and T.O.; visualization, J.L.-G. and M.E.S.; supervision, J.T.S.S. and T.O.; project administration, R.E.A. All authors have read and agreed to the published version of the manuscript.

Funding: This research received no external funding.

Data Availability Statement: The data presented in this study are available upon request from the corresponding author.

Acknowledgments: The Directorate General of Higher Education, Research and Technology (Ditjen Ristek Dikti) of the Ministry of Education, Culture, Research and Technology Indonesia is grateful for facilitating scientist mobility and paper writing during the World Class Professor (WCP) Program in 2023 (2446/E4/DT.04.03/2023). The Climate Change Impact Assessment for Local Adaptation Planning in Indonesia Program by the Ministry of Environment Agency Japan (MOEJ). Special thanks go to the Head of the Josaphat Microwave Remote Sensing Laboratory, Center for Environmental Remote Sensing, Chiba University, as a WCP collaboration partner and facility support during data analysis at Chiba University, Japan. The authors acknowledge the European Space Agency (ESA) and Alaska Satellite Facility (ASF) for providing the Sentinel-1 dataset and its dependency, the Copernicus Marine Environment Monitoring System (CMEMS) and University of Colorado for distributing sea level data, the Climate Econometrics for providing sea-level projections, the Medan City Housing and Settlement Service, Cipta Karya and Spatial Planning Office, the Ocean Fishing Port of Belawan North Sumatra Province, and IPB University for their valuable support towards the Article Processing Charges (APC). We also thank the reviewers who have provided comments and input to improve this paper.

Conflicts of Interest: The authors declare no conflicts of interest.

References

1. Church, J.A.; White, N.J. Sea-level rise from the late 19th to the early 21st century. *Surv. Geophys.* **2011**, *32*, 585–602. [CrossRef]
2. Strassburg, M.W.; Hamlington, B.D.; Leben, R.R.; Manurung, P.; Lumban-Gaol, J.; Nababan, B.; Vignudelli, S.; Kim, K.-Y. Sea level trends in Southeast Asian seas. *Clim. Past* **2015**, *11*, 743–750. [CrossRef]
3. Stammer, D.; Cazenave, A.; Ponte, R.M.; Tamisiea, M.E. Causes for contemporary regional sea level changes. *Annu. Rev. Mar. Sci.* **2013**, *5*, 21–46. [CrossRef] [PubMed]
4. Hannah, J.; Bell, R.G. Regional sea level trends in New Zealand. *J. Geophys. Res. Ocean.* **2012**, *117*, C01004. [CrossRef]
5. Nicholls, R.J.; Tol, R.S. Impacts and responses to sea-level rise: A global analysis of the SRES scenarios over the twenty-first century. *Philos. Trans. R. Soc. A Math. Phys. Eng. Sci.* **2006**, *364*, 1073–1095. [CrossRef] [PubMed]
6. Cazenave, A.; Cozannet, G.L. Sea level rise and its coastal impacts. *Earth's Future* **2014**, *2*, 15–34. [CrossRef]
7. Vitousek, S.; Barnard, P.L.; Fletcher, C.H.; Frazer, N.; Erikson, L.; Storlazzi, C.D. Doubling of coastal flooding frequency within decades due to sea-level rise. *Sci. Rep.* **2017**, *7*, 1399. [CrossRef] [PubMed]
8. Nicholls, R.J. Planning for the impacts of sea level rise. *Oceanography* **2011**, *24*, 144–157. [CrossRef]
9. Dasgupta, S.; Laplante, B.; Meisner, C.; Wheeler, D.; Yan, J. The impact of sea level rise on developing countries: A comparative analysis. *Clim. Chang.* **2009**, *93*, 379–388. [CrossRef]
10. Hinkel, J.; Lincke, D.; Vafeidis, A.T.; Perrette, M.; Nicholls, R.J.; Tol, R.S.; Marzeion, B.; Fettweis, X.; Ionescu, C.; Levermann, A. Coastal flood damage and adaptation costs under 21st century sea-level rise. *Proc. Natl. Acad. Sci. USA* **2014**, *111*, 3292–3297. [CrossRef]

11. Dutta, D. An integrated tool for assessment of flood vulnerability of coastal cities to sea-level rise and potential socio-economic impacts: A case study in Bangkok, Thailand. *Hydrol. Sci. J.* **2011**, *56*, 805–823. [CrossRef]
12. Felsenstein, D.; Lichter, M. Social and economic vulnerability of coastal communities to sea-level rise and extreme flooding. *Nat. Hazards* **2014**, *71*, 463–491. [CrossRef]
13. Sun, H.; Grandstaff, D.; Shagam, R. Land subsidence due to groundwater withdrawal: Potential damage of subsidence and sea level rise in southern New Jersey, USA. *Environ. Geol.* **1999**, *37*, 290–296. [CrossRef]
14. Erban, L.E.; Gorelick, S.M.; Zebker, H.A. Groundwater extraction, land subsidence, and sea-level rise in the Mekong Delta, Vietnam. *Environ. Res. Lett.* **2014**, *9*, 084010. [CrossRef]
15. Aucelli, P.P.C.; Di Paola, G.; Incontri, P.; Rizzo, A.; Vilardo, G.; Benassai, G.; Buonocore, B.; Pappone, G. Coastal inundation risk assessment due to subsidence and sea level rise in a Mediterranean alluvial plain (Volturno coastal plain—Southern Italy). *Estuar. Coast. Shelf Sci.* **2017**, *198*, 597–609. [CrossRef]
16. Antonioli, F.; De Falco, G.; Lo Presti, V.; Moretti, L.; Scardino, G.; Anzidei, M.; Bonaldo, D.; Carniel, S.; Leoni, G.; Furlani, S.; et al. Relative sea-level rise and potential submersion risk for 2100 on 16 coastal plains of the Mediterranean Sea. *Water* **2020**, *12*, 2173. [CrossRef]
17. Sumantyo, J.T.S.; Shimada, M.; Mathieu, P.P.; Abidin, H.Z. Long-term consecutive DInSAR for volume change estimation of land deformation. *IEEE Trans. Geosci. Remote Sens.* **2011**, *50*, 259–270. [CrossRef]
18. Abidin, H.Z.; Andreas, H.; Gumilar, I.; Wibowo, I.R.R. On correlation between urban development, land subsidence and flooding phenomena in Jakarta. *Proc. IAHS* **2015**, *370*, 15–20. [CrossRef]
19. Yastika, P.E.; Shimizu, N.; Abidin, H.Z. Monitoring of long-term land subsidence from 2003 to 2017 in coastal area of Semarang, Indonesia by SBAS DInSAR analyses using Envisat-ASAR, ALOS-PALSAR, and Sentinel-1A SAR data. *Adv. Space Res.* **2019**, *63*, 1719–1736. [CrossRef]
20. Blanco-Sánchez, P.; Mallorquí, J.J.; Duque, S.; Monells, D. The Coherent Pixels Technique (CPT): An Advanced DInSAR Technique for Nonlinear Deformation Monitoring. *Pure Appl. Geophys.* **2008**, *165*, 1167–1193. [CrossRef]
21. Casu, F.; Elefante, S.; Imperatore, P.; Zinno, I.; Manunta, M.; De Luca, C.; Lanari, R. SBAS-DInSAR Parallel Processing for Deformation Time-Series Computation. *IEEE J. Sel. Top. Appl. Earth Obs. Remote Sens.* **2014**, *7*, 3285–3296. [CrossRef]
22. Lakhote, A.; Thakkar, M.G.; Kandregula, R.S.; Jani, C.; Kothyari, G.C.; Chauhan, G.; Bhandari, S. Estimation of active surface deformation in the eastern Kachchh region, western India: Application of multi-sensor DInSAR technique. *Quat. Int.* **2021**, *575–576*, 130–140. [CrossRef]
23. Abidin, H.Z.; Andreas, H.; Djaja, R.; Darmawan, D.; Gamal, M. Land subsidence characteristics of Jakarta between 1997 and 2005, as estimated using GPS surveys. *GPS Solut.* **2008**, *12*, 23–32. [CrossRef]
24. Stramondo, S.; Saroli, M.; Tolomei, C.; Moro, M.; Doumaz, F.; Pesci, A.; Loddo, F.; Baldi, P.; Boschi, E. Surface movements in Bologna (Po plain—Italy) detected by multitemporal DInSAR. *Remote Sen. Environ.* **2007**, *110*, 304–316. [CrossRef]
25. Di Martire, D.; Novellino, A.; Ramondini, M.; Calcaterra, D. A-differential synthetic aperture radar interferometry analysis of a deep seated gravitational slope deformation occurring at Bisaccia (Italy). *Sci. Total Environ.* **2016**, *550*, 556–573. [CrossRef] [PubMed]
26. Nishi, K.; Sumantyo, J.T.S.; Kawai, M.; Waqar, M.M.; Chen, X. Monitoring of land deformation in Kanagawa Prefecture using GNSS and C-band Sentinel-1 based consecutive DInSAR. *J. Instrum. Autom. Syst.* **2021**, *7*, 12–21.
27. Bayuaji, L.; Sumantyo, J.T.S.; Kuze, H. ALOS PALSAR D-InSAR for land subsidence mapping in Jakarta, Indonesia. *Can. J. Remote Sens.* **2010**, *36*, 1–8. [CrossRef]
28. Mohammed, O.I.; Saeidi, V.; Pradhan, B.; Yusuf, Y.A. Advanced differential interferometry synthetic aperture radar techniques for deformation monitoring: A review on sensors and recent research development. *Geocarto Int.* **2014**, *29*, 536–553. [CrossRef]
29. Tarigan, A.P.M.; Zevri, A.; Iskandar, R.; Indrawan, I. A study on the estimation of flood damage in Medan city. In Proceedings of the 6th International Conference of Euro Asia Civil Engineering Forum (EACEF 2017), Seoul, Republic of Korea, 22–25 August 2017; MATEC Web of Conferences. EDP Sciences: Les Ulis, France, 2017; Volume 138. Available online: https://www.matec-conferences.org/articles/matecconf/abs/2017/52/matecconf_eacef2017_06010/matecconf_eacef2017_06010.html (accessed on 7 September 2023).
30. Hutapea, S. Assessment of deli watershed flood that caused some damage in Medan City, Indonesia. *J. Rangel. Sci.* **2019**, *9*, 300–312. Available online: https://journals.iau.ir/,article_665329_8c0fca2a77ce98058945ede578be3923.pdf (accessed on 15 October 2023).
31. Dian, R.; Lismawaty, L.; Pinem, D.E.; Sianipar, B.B. Flood vulnerability and flood-prone area map at Medan City, Indonesia. *IOP Conf. Ser. Earth Environ. Sci.* **2018**, *200*, 012039. [CrossRef]
32. Tempa, K. District flood vulnerability assessment using analytic hierarchy process (AHP) with historical flood events in Bhutan. *PLoS ONE* **2022**, *17*, e0270467. [CrossRef] [PubMed]
33. Ouma, Y.O.; Tateishi, R. Urban flood vulnerability and risk mapping using integrated multi-parametric AHP and GIS: Methodological overview and case study assessment. *Water* **2014**, *6*, 1515–1545. [CrossRef]
34. Kwan, S.C.; Saragih, I.J. Urban environment and cause specific visits to community health centers of Medan city, Indonesia. *Sustain. Cities Soc.* **2021**, *59*, 102228. [CrossRef]
35. Ullo, S.L.; Addabbo, P.; Di Martire, D.D.; Sica, S.; Fiscante, N.; Cicala, L.; Angelino, C.V. Application of DInSAR technique to high coherence Sentinel-1 images for dam monitoring and result validation through in situ measurements. *IEEE J. Sel. Top. Appl. Earth Obs. Remote Sens.* **2019**, *12*, 875–890. [CrossRef]

36. Jevrejeva, S.; Jackson, L.P.; Riva, R.E.M.; Grinsted, A.; Moore, J.C. Coastal Sea Level Rise with Warming above 2 °C. *Proc. Natl. Acad. Sci. USA* **2016**, *113*, 13342–13347. [CrossRef]
37. Jackson, L.P.; Jevrejeva, S. A Probabilistic Approach to 21st Century Regional Sea-Level Projections Using RCP and High-End Scenarios. *Glob. Planet. Chang.* **2016**, *146*, 179–189. [CrossRef]
38. Tampubolon, K. Aplikasi Sistem Informasi Geografis (SIG) sebagai Penentuan kawasan Rawan banjir di Kota Medan. *J. Pembang. Perkota.* **2018**, *6*, 63–68, (In Bahasa Indonesia). Available online: https://www.researchgate.net/profile/KokoTampubolon/publication/330934511_APLIKASI_SISTEM_INFORMASI_GEOGRAFIS_SIG_SEBAGAI_PENENTUAN_KAWASAN_RAWAN_BANJIR_DI_KOTA_MEDAN/links/5c5c5085299bf1d14cb33832/APLIKASI-SISTEM-INFORMASI-GEOGRAFIS-SIG-SEBAGAI-PENENTUAN-KAWASAN-RAWAN-BANJIR-DI-KOTA-MEDAN.pdf (accessed on 5 September 2023).
39. Papathoma, M.; Dominey-Howes, D.; Zong, Y.; Smith, D. Assessing tsunami vulnerability, an example from Herakleio, Crete. *Nat. Hazard Earth Sys. Sci.* **2003**, *3*, 377–389. [CrossRef]
40. Saaty, T.L. A scaling method for priorities in hierarchical structures. *J. Math. Psychol.* **1977**, *15*, 234–281. [CrossRef]
41. Saaty, T.L. Decision making—The analytic hierarchy and network processes (AHP/ANP). *J. Syst. Sci. Syst. Eng.* **2004**, *13*, 1–35. [CrossRef]
42. Chen, X.; Zhang, X.; Church, J.A.; Watson, C.S.; King, M.A.; Monselesan, D.; Legresy, B.; Harig, C. The increasing rate of global mean sea-level rise during 1993–2014. *Nat. Clim. Chang.* **2017**, *7*, 492–495. [CrossRef]
43. Fasullo, J.T.; Nerem, R.S. Altimeter-era emergence of the patterns of forced sea-level rise in climate models and implications for the future. *Proc. Natl. Acad. Sci. USA* **2018**, *115*, 12944–12949. [CrossRef] [PubMed]
44. Lumban-Gaol, J.; Vignudelli, S.; Nurjaya, I.W.; Natih, N.M.N.; Sinurat, M.E.; Arhatin, R.E.; Kusumaningrum, E.E. Evaluation of altimetry satellite data products and sea level trends in the Indonesian maritime continent. *IOP Conf. Ser. Earth Environ. Sci.* **2021**, *944*, 012041. [CrossRef]
45. Handoko, E.Y.; Fernandes, M.J.; Lázaro, C. Assessment of altimetric range and geophysical corrections and mean sea surface models—Impacts on sea level variability around the Indonesian seas. *Remote Sens.* **2017**, *9*, 102. [CrossRef]
46. Nugroho, H.; Rinaldy. Pemetaan Undulasi Kota Medan Menggunakan Hasil Pengukuran Tinggi Tahun 2010. *J. Itenas Rekayasa* **2013**, *17*. (In Bahasa Indonesia). Available online: https://ejurnal.itenas.ac.id/index.php/rekayasa/article/view/471/637 (accessed on 5 July 2023).
47. Hermon, D. *Geografi Bencana Alam*, 1st ed.; Rajawali Pers: Jakarta, Indonesia, 2015; ISBN 978-979-769-820-1. (In Bahasa Indonesia).
48. Gornitz, V.M.; White, T.W.; Daniels, R.C. *A Coastal Hazards Data Base for the US East Coast*; Oak Ridge National Lab.: Oak Ridge, TN, USA, 1992.
49. Pendleton, E.A.; Thieler, E.R.; Williams, S.J. Importance of coastal change variables in determining vulnerability to sea- and lake-level change. *J. Coast. Res.* **2010**, *261*, 176–183. [CrossRef]
50. Zain, A.F.M. Distribution, Structure and Function of Urban Green Space in Southeast Asian Megacities with Special Reference to Jakarta Metropolitan Region (JABOTABEK). Doctoral Dissertation, Tokyo University, Tokyo, Japan, 2002. Available online: https://ci.nii.ac.jp/naid/500000245635/ (accessed on 10 October 2023).
51. Church, J.A.; Clark, P.U.; Cazenave, A.; Gregory, J.M.; Jevrejeva, S.; Levermann, A.; Merrifield, M.A.; Milne, G.A.; Nerem, R.S.; Nunn, P.D.; et al. Chapter 13: Sea level change. In *Climate Change, 2013: The Physical Science Basis: Contribution of Working Group I to the Fifth Assessment Report of the Intergovernmental Panel on Climate Change*; Cambridge University Press: Cambridge, UK; New York, NY, USA, 2013.
52. Mancini, F.; Grassi, F.; Cenni, N. A workflow based on SNAP–StaMPS open-source tools and GNSS data for PSI-based ground deformation using dual-orbit sentinel-1 data: Accuracy assessment with error propagation analysis. *Remote Sens.* **2021**, *13*, 753. [CrossRef]
53. Wang, J.; Yi, S.; Li, M.; Wang, L.; Song, C. Effects of sea level rise, land subsidence, bathymetric change and typhoon tracks on storm flooding in the coastal areas of Shanghai. *Sci. Total Environ.* **2018**, *621*, 228–234. [CrossRef]
54. Anzidei, M.; Bosman, A.; Carluccio, R.; Casalbore, D.; D'Ajello Caracciolo, F.; Esposito, A.; Nicolosi, I.; Pietrantonio, G.; Vecchio, A.; Carmisciano, C.; et al. Flooding scenarios due to land subsidence and sea-level rise: A case study for Lipari Island (Italy). *Terra Nova* **2017**, *29*, 44–51. [CrossRef]
55. Rocha, C.; Antunes, C.; Catita, C. Coastal vulnerability assessment due to sea level rise: The case study of the Atlantic coast of mainland Portugal. *Water* **2020**, *12*, 360. [CrossRef]
56. Scardino, G.; Anzidei, M.; Petio, P.; Serpelloni, E.; De Santis, V.; Rizzo, A.; Liso, S.I.; Zingaro, M.; Capolongo, D.; Vecchio, A.; et al. The impact of future sea-level rise on low-lying subsiding coasts: A case study of tavoliere delle puglie (Southern Italy). *Remote Sens.* **2022**, *14*, 4936. [CrossRef]